processes

MDPI

Article

Numerical Investigation on Heat Transfer of Supercritical CO_2 in Minichannel with Fins Integrated in Sidewalls

Lei Chai

Centre for Sustainable Energy Use in Food Chain (CSEF), Brunel University London, Uxbridge UB8 3PH, Middlesex, UK; lei.chai@brunel.ac.uk; Tel.: +44-1895-265834

Abstract

Gas coolers play a critical role in CO_2 refrigeration and heat pump systems, where their thermohydraulic characteristics substantially influence the overall system performance. To improve the heat transfer performance of gas coolers, minichannels with aligned or offset fins integrated in the channel sidewalls are proposed to enlarge the heat transfer surface and intensify the flow turbulence. Unlike conventional refrigerants, supercritical CO_2 exhibits significant variations in thermophysical properties with temperature changes, which results in distinct heat transfer behavior. Three-dimensional numerical models are therefore purposely developed by employing the Shear Stress Transport k-ω turbulent model and including the entrance region effect, NIST real-gas thermophysical properties and buoyancy effect. A constant heat flux boundary is employed on the four-side channel walls to ensure that the temperature of CO_2 flowing in the channel exactly decreases from 373.15 K to 308.15 K. The results show that the fins integrated in the channel sidewalls can significantly improve the heat transfer performance, and the heat transfer coefficient significantly increases with increasing mass flux. Compared to the reference smooth channel, the heat transfer performance is enhanced by a factor of 1.85–2.15 with aligned fins and 1.44–1.61 with offset fins.

Keywords: numerical simulation; heat transfer; supercritical CO_2; minichannel gas cooler

Academic Editors: Qian Li, Jue Wang and Wenke Zheng

Received: 29 July 2025
Revised: 17 August 2025
Accepted: 18 August 2025
Published: 20 August 2025

Citation: Chai, L. Numerical Investigation on Heat Transfer of Supercritical CO_2 in Minichannel with Fins Integrated in Sidewalls. *Processes* **2025**, *13*, 2630. https://doi.org/10.3390/pr13082630

1. Introduction

With rising environmental concerns, CO_2 has gained in prominence as a natural refrigerant due to its minimal direct impact on climate change. Unlike ammonia or hydrocarbons, CO_2 is also safe in well-designed systems. It is considered a strong candidate to replace harmful synthetic refrigerants, such as chlorofluorocarbons (CFCs) and hydrochlorofluorocarbons (HCFCs), which contribute to ozone layer depletion. Additionally, since CO_2 can be sourced from industrial byproducts, its use in refrigeration systems results in a net-zero climate impact and contributes to lowering greenhouse gas emissions. It is also cost-effective and widely accessible, and it has shown competitive performance compared to conventional refrigerants [1,2].

Since Lorentzen's patent application for a trans-critical CO_2 automotive air conditioning system in the early 1990s [3], the use of CO_2 in refrigeration, air conditioning and heat pump systems has attracted significant research interest. In trans-critical CO_2 cycles, two factors require special attention: One is CO_2's thermophysical properties; it has a low critical temperature of 31.1 °C and a high working pressure of 73.7 bar. The other is the heat exchangers used for gas coolers and evaporators, which account for nearly half of the mass and form a major part of the volume of such systems, and their performance directly

impacts the system efficiency [4]. To enhance system compactness, very-small-diameter tubes are required, along with thick walls to tolerate pressures up to 140 bar, which complicates the manufacturing process. Therefore, enhancing the heat transfer performance of gas coolers and evaporators is crucial to reducing compressor energy consumption and simplifying fabrication, ultimately lowering both manufacturing and operating costs.

Gas coolers are generally classified into air-cooled and water-cooled types, depending on the cooling medium used, and the choice of coolant significantly influences the design and configuration of the heat exchanger [5]. In air-cooled CO_2 gas coolers, commonly adopted configurations include finned-tube and microchannel-tube finned heat exchangers. Pettersen et al. [4] evaluated the performance of compact heat exchangers and reported that microchannel-tube designs offer superior efficiency compared to traditional round-tube exchangers. These designs not only reduce the physical size for a given thermal duty but also handle high operating pressures effectively. Yin et al. [6] developed a first principles-based model for microchannel-tube finned gas coolers and examined various layout configurations within fixed packaging dimensions and concluded that employing the multiple slab arrangements notably enhanced heat transfer. Asinari et al. [7] proposed a detailed three-dimensional (3D) simulation model for the microchannel-tube finned gas coolers and highlighted the influence of thermal conduction through fins and tube walls. Their analysis showed that the longitudinal conduction in fins and the transverse and the longitudinal conduction in tubes had minimal impact on the overall heat transfer and on the temperature distribution. Ge et al. [8], Gupta et al. [9], Marcinichen et al. [10] and Chai et al. [11] proposed detailed mathematical models for finned-tube gas coolers based on the segment-by-segment design and investigated their thermohydraulic performance operating with refrigerant pressures near the critical point. Generally, the microchannel configurations with integrated fins significantly enhance the surface area and heat transfer performance and make them well-suited for the compact system designs. These exchangers also reduce the refrigerant charge, system weight and overall footprint. However, air-cooled heat exchangers face certain limitations, primarily due to CO_2's unique thermophysical properties and the challenges of air-side heat transfer. Air is a poor heat transfer fluid due to its low thermal conductivity and low specific heat compared to water or refrigerants, and air-cooled gas coolers require large surface areas to achieve sufficient heat rejection and make them bulky. Mismatch with air cooling leads to pinch points and reduced effectiveness, with most of the CO_2 temperature drop occurring in a very short section of the exchanger. Additional drawbacks include higher flow resistance due to narrow channels and performance deterioration under elevated ambient temperatures. Material selection, corrosion resistance and ease of maintenance are also key factors when designing air-cooled CO_2 systems.

In water-cooled gas coolers, the pinch point issue is notably less severe due to the similar specific heat capacity and density between water and supercritical CO_2. The temperature glide during heat rejection aligns well with water heating applications. Water's high specific heat capacity also allows it to absorb and transfer substantial thermal energy with minimal temperature variation, which makes water-based precoolers more effective than their air-cooled counterparts. This improved thermal performance reduces the energy demand of the cooling process and further leads to energy savings and improved overall system efficiency. Several water-coupled gas cooler configurations have been explored, including brazed plate heat exchangers, printed circuit heat exchangers (PCHEs), fluted tube-in-tube heat exchangers, serpentine microchannel exchangers and multi-twisted-tube designs. Plate-type heat exchangers enhance heat transfer by promoting turbulence and offering a large surface area, which allows for more compact designs. Zendehboudi et al. [12] conducted experimental studies on brazed plate heat exchangers using supercritical CO_2

for domestic water and space heating applications and concluded that thermal resistance on the CO_2 side predominantly limits the total heat transfer. PCHEs have an exceptionally high heat transfer rate due to their microchannel design and improve the heat transfer performance by their increased heat transfer area, the constantly disrupted boundary layers and the augmented fluid turbulence. Chu et al. [13] experimentally investigated the thermo-hydraulic behavior of PCHEs with zigzag channels between supercritical CO_2 and water at pressures that ranged from 80 bar to 110 bar. They found that convective thermal resistance on the CO_2 side had the most significant impact, and the gas cooler performance was more sensitive to changes in CO_2 flow rate than that of water. Ren et al. [14] numerically investigated the local flow and heat transfer performance of supercritical CO_2 in horizontal semicircular zigzag channels near the critical and pseudo-critical points. They analyzed how mass flux and geometric parameters like pitch and inclination angle affect heat transfer performance. Fluted tube-in-tube exchangers, composed of a corrugated inner tube nested within a smooth outer tube, promote internal fluid mixing and outperform smooth tube designs in heat transfer efficiency. Zhu et al. [15] investigated the heat transfer characteristics of supercritical CO_2 in two fluted tube-in-tube gas coolers and a smooth tube-in-tube gas cooler and demonstrated that the overall heat transfer coefficients of the fluted tubes are 2–3 times that of the smooth tube. Ye et al. [16] studied the heat transfer performance of a fluted tube-in-tube gas cooler in a trans-critical CO_2 heat pump water heater and showed that the fluted tube-in-tube gas cooler had higher heat transfer capacity in most conditions. The serpentine microchannel heat exchangers consist of a microchannel tube bent into a serpentine shape with fins and connection pipes integrally brazed together. This design maximizes surface area and thermal performance. Fronk and Garimella [17,18] investigated this configuration and developed a predictive model to optimize its performance across various operating scenarios. Multi-twisted-tube exchangers incorporate helically twisted tubes to enhance surface area and promote turbulence. Yang et al. [19] explored the thermohydraulic performance of these exchangers and examined how varying the number of inner tubes impacts heat transfer and pressure loss. Their findings highlighted the need to optimize gas cooler design for both system efficiency and water outlet temperatures. Generally, water-coupled gas coolers offer numerous advantages, including high heat transfer rates, compact size, flexible thermal control and ease of integration into confined or pre-existing systems. Their efficiency and compactness make them particularly suitable for space-constrained or modular applications.

Based on the heat transfer enhancement mechanisms mentioned above, minichannel gas coolers integrating aligned or offset fins in the channel sidewalls are proposed with the purpose of further reducing the thermal resistance on the CO_2 side. The minichannel design is expected to increase the heat transfer surface area and reduce the heat exchanger weight and the refrigerant charge. The fins are expected to promote turbulence within the fluid flow and enhance the fluid mixing. In the design of innovative supercritical CO_2 gas coolers, 3D computational fluid dynamics (CFD) simulations have become a powerful tool to predict the heat exchanger performance. By resolving the detailed velocity and temperature fields within complex geometries, 3D CFD allows for precise prediction of local and average heat transfer and fluid flow performance, providing insights that are difficult to achieve experimentally. It allows for the accurate visualization of flow structures, including secondary flows, recirculation zones and boundary layer development. This is crucial for understanding how geometric modifications disrupt the near-wall laminar layer and promote turbulence, which directly enhances convective heat transfer. CFD also provides a detailed mapping of temperature fields throughout the channel, capturing the effect of fin configurations on the local temperature difference between the fluid bulk and the channel walls. This enables optimization of fin design to achieve maximum heat transfer

without excessive pressure drop. Therefore, 3D CFD simulation has been employed to investigate the thermohydraulic performance of the minichannel gas coolers proposed in this study. Furthermore, near the critical point, supercritical CO_2 exhibits drastic changes in properties such as density, specific heat, thermal conductivity and viscosity with even small temperature or pressure variations (as shown in Figure 1). Accordingly, the NIST real-gas thermophysical properties have been linked to the solver to dynamically call property data during iterations rather than relying on simplified equations or static tables.

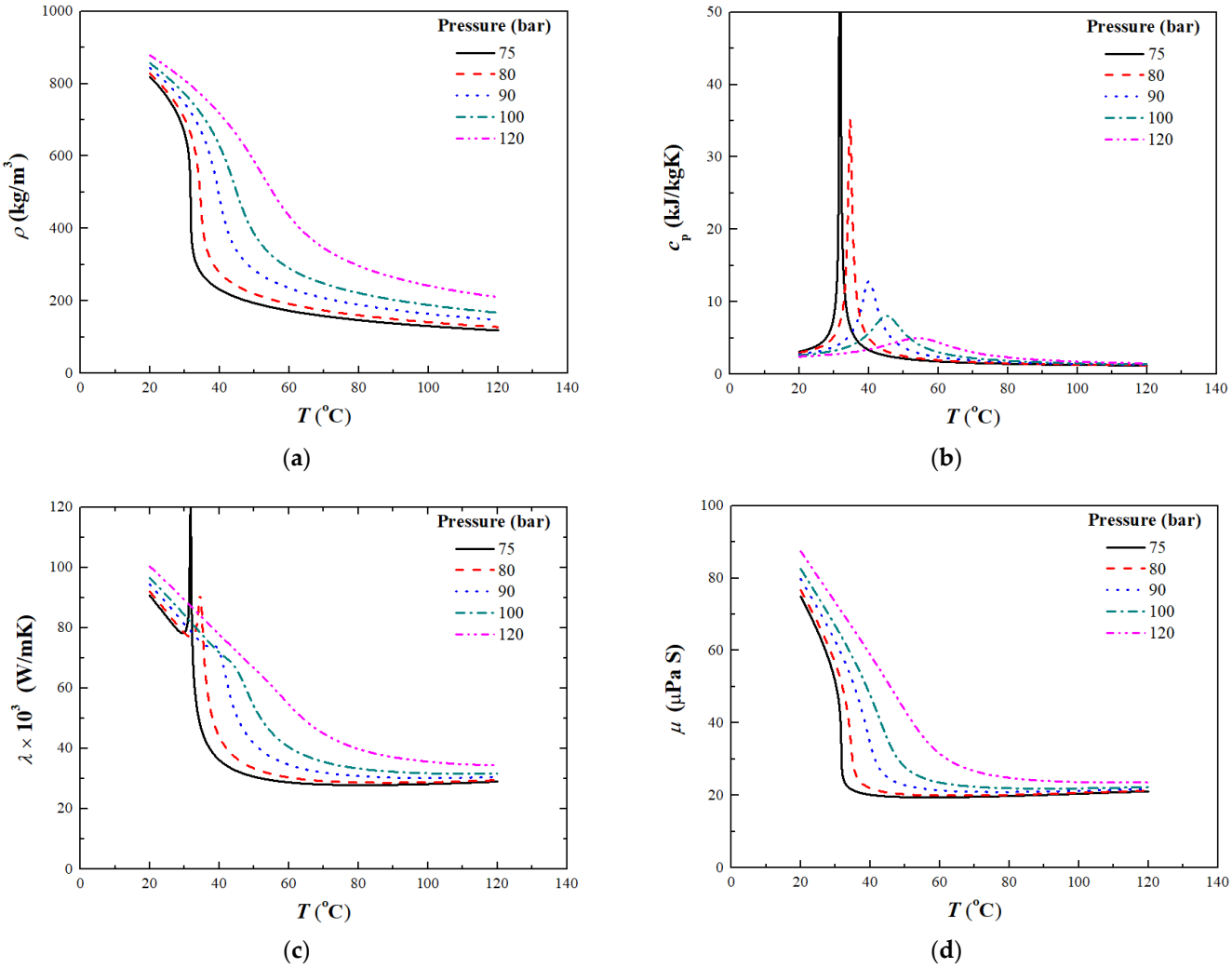

Figure 1. Thermophysical properties of CO_2. (**a**) Density; (**b**) Specific heat; (**c**) Thermal conductivity; (**d**) Dynamic viscosity.

2. Numerical Model and Solution Method

2.1. Computational Domain and Geometric Configurations

When modeling supercritical CO_2 flow in minichannel gas coolers, simplifying the domain to a single representative channel is a common and computationally efficient approach if the minichannel array is uniformly distributed. The single representative channels employed in this study are shown in Figure 2, one with aligned fin arrangement and the other offset. The rectangular channel has a width of 1 mm and height of 1.5 mm. The length of the channel is 200 mm. The fins are embedded in the two channel sidewalls. Drop-shaped pin fins have demonstrated significant improvements in heat transfer performance over traditional circular fins by effectively increasing flow turbulence and enhancing fluid mixing and controlling vortex shedding [20,21]. The fin geometry integrated into

the channel walls is thus inspired by the drop-shaped design and is constructed using a combination of a quarter-circle and a right-angled triangle for simplicity and effectiveness. The radius of the circle is 0.25 mm and the two legs of the triangle are 0.25 mm and 0.5 mm long. Consequently, the integrated fins have a height of 1.5 mm, width of 0.25 mm and length of 0.75 mm. The stream-wise fin spacing on the same sidewall is 4 mm. Meanwhile, a smooth minichannel with width of 1 mm and height 1.5 mm is introduced for comparison and as a reference. The selection of the dimensions of the fins ensures the proposed channels have exactly the same surface area as the reference smooth channel (1000 mm^2).

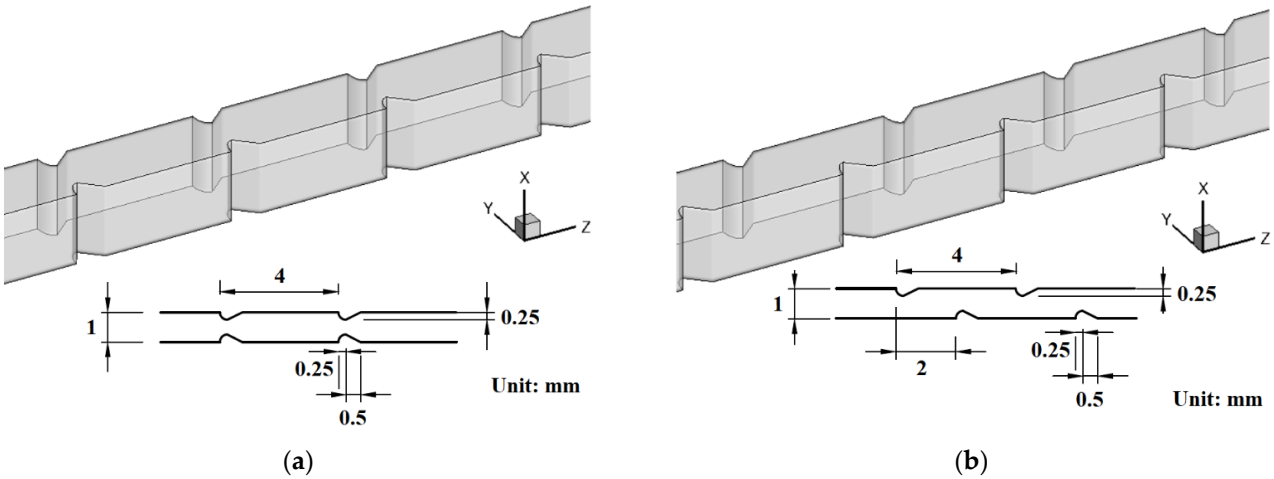

(**a**) (**b**)

Figure 2. Geometric configuration of the channels with fins in sidewalls. (**a**) Channel with aligned fins; (**b**) Channel with offset fins.

2.2. Governing Equations and Boundary Conditions

The three-dimensional numerical simulations are based on the following key assumptions: the flow is steady-state and turbulent; CO_2 enters the channel with a uniform velocity and temperature profile; real-gas thermophysical properties from the NIST database are used to account for the significant variations in CO_2 properties near the critical and pseudo-critical regions; both entrance effects and buoyancy influences are taken into consideration. The following governing equations are used in mathematical modeling.

Continuity:

$$\frac{\partial}{\partial x_i}(\rho u_i) = 0 \tag{1}$$

Momentum:

$$\frac{\partial}{\partial x_i}(\rho u_i u_j) = \rho g_j - \frac{\partial p}{\partial x_j} + \frac{\partial}{\partial x_i}\left[\mu\left(\frac{\partial u_j}{\partial x_i} + \frac{\partial u_i}{\partial x_j}\right) + \mu_t\left(\frac{\partial u_j}{\partial x_i} + \frac{\partial u_i}{\partial x_j}\right) - \frac{2}{3}\rho k\delta_{ij}\right] \tag{2}$$

Energy:

$$\frac{\partial}{\partial x_i}(\rho u_i c_p T) = \frac{\partial}{\partial x_i}\left(\lambda\frac{\partial T}{\partial x_i}\right) \tag{3}$$

where u is the fluid velocity vector, p is the pressure, ρ, μ, c_p, and λ are the density, dynamic viscosity, specific heat capacity and thermal conductivity of fluid, respectively.

The integration of fins into channel sidewalls significantly changes the flow velocity, direction and thermal boundary layer development of supercritical CO_2. These modifications introduce complex fluid–structure interactions that must be carefully modeled to predict thermohydraulic performance accurately. Furthermore, near-wall accuracy is also crucial when strong property gradients, flow separation and secondary flows occur, as in channels with fins or abrupt geometry changes. Therefore, the Shear Stress Transport

(SST) k-ω model has been employed in the current numerical simulations. The SST k-ω turbulence model offers distinct advantages for simulating turbulent flows with changing velocity and flow directions, which makes it highly suitable for complex heat exchanger and channel flow applications, by combining the benefits of the k-ω formulation near walls with the k-ε formulation in the free-stream region. It is also strongly recommended for the simulation of supercritical turbulence flow with changed flow velocity and flow directions by Ren et al. [14] and Bai et al. [22].

$$\frac{\partial}{\partial x_i}(\rho k u_i) = \frac{\partial}{\partial x_j}\left[\Gamma_k \frac{\partial k}{\partial x_j}\right] + G_k - Y_k + S_k \tag{4}$$

$$\frac{\partial}{\partial x_i}(\rho \omega u_i) = \frac{\partial}{\partial x_i}\left[\Gamma_\omega \frac{\partial \omega}{\partial x_j}\right] + G_\omega - Y_\omega + D_\omega + S_\omega \tag{5}$$

where G_k represents the generation of turbulence kinetic energy due to mean velocity gradients and G_ω represents the generation of ω, Γ_k and Γ_ω are the effective diffusivity of k and ω, Y_k and Y_ω represent the dissipation of k and ω due to turbulence, D_ω represents the cross-diffusion term and S_k and S_ω are the user-defined source terms ε, respectively.

For the sake of completeness, the boundary conditions are illustrated as follows. The mass-flow inlet boundary condition is applied at the channel inlet, and the pressure outlet at the channel outlet. The inlet mass flow rate varies from 0.0005 kg/s to 0.003 kg/s, the corresponding CO_2 inlet temperature is 373.15 K and the outlet pressure is fixed at 100 bar. Constant heat flux boundary is employed for the four-side channel walls. For each mass flow rate, the constant heat flux is calculated to ensure the CO_2 flowing through the channels exactly decreases from 373.15 K to 308.15 K. The employed heat fluxes for each mass flow rate are shown in Table 1. The based CO_2 temperature range of 308.15–373.15 K in the channel is directly related to the trans-critical CO_2 refrigeration and heat pump operation.

Table 1. Employed heat fluxes for each mass flow rate.

m, kg/s	0.0005	0.001	0.0015	0.002	0.0025	0.003
q, W/m^2	−107,310	−214,620	−321,930	−429,240	−536,550	−643,860

2.3. Solution Methods and Data Acquisition

During the simulation, ANSYS Fluent 2019 R1 is employed to solve the governing equations of the model. The SIMPLEC scheme is adopted for solving the coupled differential equations related to velocity, pressure and energy within each control volume. To discretize the convection terms, a second-order upwind method is utilized. The NIST real-gas thermophysical properties of supercritical CO_2 are realized by activating and dynamically loading the software REFPROP v9.1 into the solver Fluent. After activation, REFPROP takes over the computation of all relevant thermophysical properties and ensures that property evaluations are handled directly by the database rather than the default Fluent routines. The solutions are converged when the normalized residual values are less than 10^{-5} for all the variables. For each channel, a grid independence test is performed using several different mesh sizes, as shown in Table 2. The heat transfer coefficient and pressure drop become more stabilized as the grid number increases. For the channel with aligned fins, the difference is less than 1.0% between the grid numbers 1.668 million and 3.335 million for both the heat transfer coefficient and pressure drop. Therefore, the grid number 1.668 million is selected for the simulation of the channel with aligned fins. Correspondingly, the grid number 1.667 million is selected for the channel with offset fins. For

accurate calculation of the boundary layer, the mesh near the channel walls is refined as shown in Figure 3.

Table 2. Grid independence test.

Cell Number, Million	$p_{in} - p_{out}$, (kPa)	$\overline{h}$, (kW/(m^2·K))
Channel with aligned fins		
0.319	31.59	12.66
0.638	30.24	12.18
1.668	29.06	11.83
3.335	28.91	11.77
Channel with offset fins		
0.319	17.02	9.65
0.637	16.30	9.29
1.667	15.51	8.93
3.334	15.36	8.84

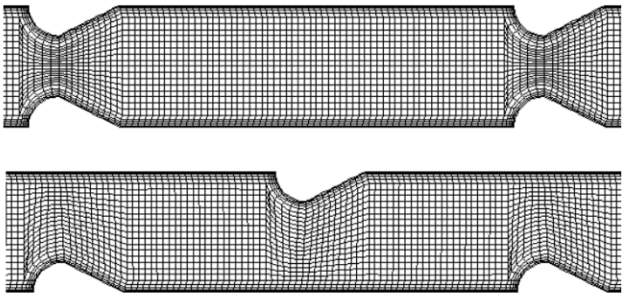

Figure 3. Grid generations in the y–z plane (x = 0.75 mm).

To present the numerical results of supercritical CO_2 flowing in the channels, the important parameters are given below.

Local Reynolds number:

$$Re_z = \frac{GD}{\mu_z} \tag{6}$$

Local heat transfer coefficient:

$$h_z = \frac{q_z}{\left|T_{w,z} - T_{f,z}\right|} = \frac{q_z}{\Delta T_z} \tag{7}$$

Local Nusselt number:

$$Nu_z = \frac{h_z D}{\lambda_{f,z}} \tag{8}$$

Local friction factor:

$$f_z = \frac{2\rho_z D}{G^2}\frac{dp_f}{dz} \tag{9}$$

Average Reynolds number:

$$\overline{Re} = \frac{\int_0^L Re_z dz}{L} \tag{10}$$

Average heat transfer coefficient:

$$\overline{h} = \frac{\int_0^L h_z dz}{L} \tag{11}$$

Average Nusselt number:

$$\overline{Nu} = \frac{\int_0^L Nu_z dz}{L} \tag{12}$$

Average friction factor:

$$\overline{f} = \frac{\int_0^L f_z dz}{L} \tag{13}$$

where G is the mass flux, D is the hydraulic diameter, L is the channel length. The local heat flux, local wall temperature and local fluid temperature at a fixed z plane are denoted by q_z, $T_{w,z}$ and $T_{f,z}$, respectively. The ρ_z, μ_z and $\lambda_{f,z}$ represent the local density, dynamic viscosity and thermal conductivity of supercritical CO_2, respectively. The $\frac{dp_f}{dz}$ is the pressure gradient due to the friction. The pressure variation due to the flow acceleration and deceleration caused by the density change are eliminated during the calculation of friction factors.

3. Model Validation

To verify the accuracy of the developed numerical model, simulation results are compared against established empirical correlations. For supercritical CO_2 flow in minichannels, Chai and Tassou [23] evaluated various empirical models and concluded that the correlation proposed by Krasnoshchekov and Protopopov [24] provided the most reliable predictions under both heating and cooling conditions. Jackson [25] reviewed heat transfer correlations for supercritical CO_2 and again identified the Krasnoshchekov–Protopopov correlation as the most effective. This correlation was proposed for forced convective heat transfer of supercritical CO_2 from their experimental results:

$$Nu = Nu_0 \left(\frac{\rho_w}{\rho_b}\right)^{0.3} \left(\frac{\overline{c_p}}{c_{pb}}\right)^n \tag{14}$$

$$Nu_0 = \frac{(f/8) Re_b \overline{Pr}_b}{12.7\sqrt{f/8}\left(\overline{Pr}_b^{2/3} - 1\right) + 1.07} \tag{15}$$

$$f = \frac{1}{\left(1.82 log_{10} Re_b - 1.64\right)^2} \tag{16}$$

where the exponent n depends on CO_2 bulk temperature and channel wall temperature. The $\overline{c_p}$ and $\overline{Pr}_b$ are, respectively, the averaged specific heat and Prandtl number over cross-section at constant pressure. Accordingly, this correlation is adopted for validating the current simulated heat transfer results. For friction factor validation, the well-known Petukhov correlation [26] (as shown in Equation (16)), recognized for its reliability in predicting turbulent flow behavior, is employed.

Figure 4 shows a comparison between the numerical results and the empirical predictions from above correlations. Given the complex behavior of supercritical CO_2 near the critical and pseudo-critical regions and small size of the employed minichannel, the comparison shows good agreement, which confirms the validity and accuracy of the numerical modeling approach and solution methodology used in this study.

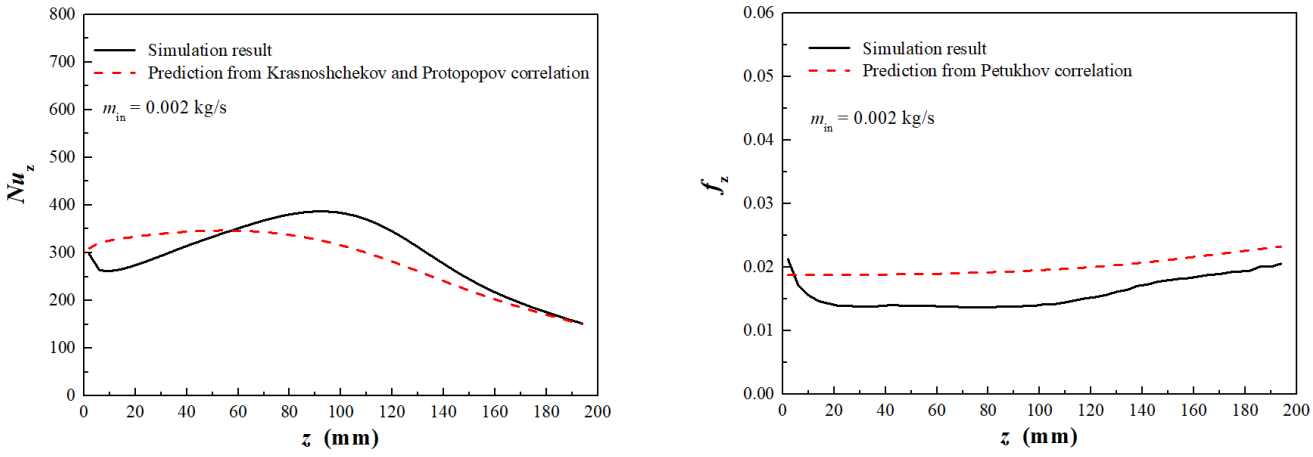

Figure 4. Comparison of simulation results with predictions from empirical correlations. (**a**) Local Nusselt number; (**b**) Local friction factor.

4. Results and Discussion

4.1. Velocity Contour and Temperature Field

The velocity contour and temperature field of supercritical CO_2 flowing in minichannels are crucial for understanding and optimizing heat transfer performance. The velocity contour illustrates how the fluid accelerates or decelerates along the channel, particularly in the near-wall regions, where no-slip boundary conditions create velocity gradients. This distribution is essential for identifying flow development regions, boundary layer behavior and areas of turbulence, all of which influence the convective heat transfer coefficient. The temperature field reveals how heat is distributed within the fluid and how thermal gradients evolve along the flow direction. For supercritical CO_2, which exhibits strong variations in thermophysical properties near the pseudo-critical point, the temperature field becomes especially important. Sharp changes in specific heat capacity and thermal conductivity can significantly affect local heat transfer coefficients. The interaction between the velocity contour and temperature field determines the efficiency of heat transfer. Understanding these fields together allows for detailed thermohydraulic analysis and helps in the design of more compact and efficient minichannel heat exchangers for supercritical CO_2 applications. Therefore, the velocity contour and the temperature field are illustrated first.

Three cross-sections near the middle of the channel are selected at z = 98 mm, 100 mm and 102 mm, respectively, as indicated in Figure 5, to cover a periodical variation of the flow passage. The local velocity contours for the mass flow rate of 0.001 kg/s are shown by Figures 6–8 for the smooth channel, the channel with aligned fins and the channel with offset fins, respectively. In the smooth channel, the flow velocity is highest at the center and significantly lower near the walls, particularly in the corner regions. In addition, as CO_2 is cooled, its density increases, which leads to a gradual decrease in flow velocity along the channel. Aligned and offset fin configurations in microchannel sidewalls both aim to improve heat transfer by promoting turbulence, enhancing fluid mixing and disrupting the thermal boundary layer, but they achieve these effects through different mechanisms and to varying extents. In aligned fin configurations, fins are positioned directly opposite each other along the sidewalls, which create a periodically varying but symmetric flow passage. This arrangement forces the supercritical CO_2 to accelerate and decelerate in a predictable pattern as it passes through narrow and wide sections. The symmetry leads to strong flow constriction and expansion, and generates high turbulence intensity near the fins. As a result, the aligned fins are more effective in consistently breaking up the

boundary layer along the flow path, which leads to greater mixing between the near-wall fluid and the channel core. This often results in higher heat transfer coefficients compared to offset fins. Offset fin configurations, on the other hand, stagger the fin positions along the sidewalls and create an asymmetric and more complex flow path. This design induces frequent changes in flow direction and promotes additional lateral mixing and secondary vortices. While the boundary layer disruption is still significant, it is generally less uniform compared to the aligned configuration, which leads to slightly lower turbulence intensity but potentially reduced pressure drops.

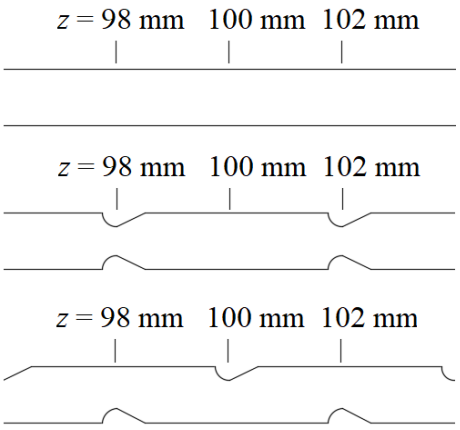

Figure 5. Location of three selected cross-sections to show velocity and temperature distribution.

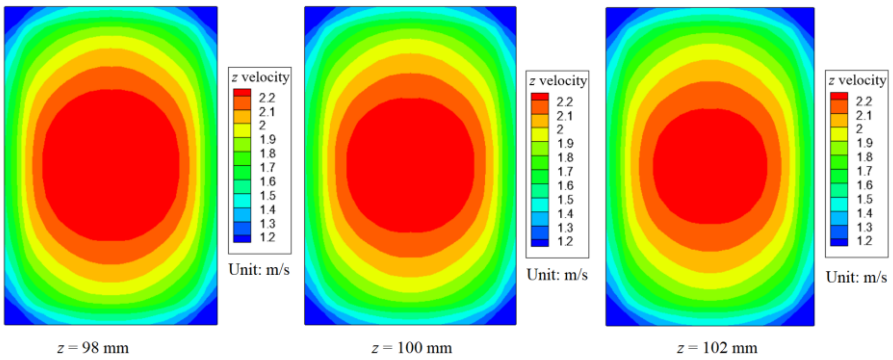

Figure 6. Velocity contours of the smooth channel.

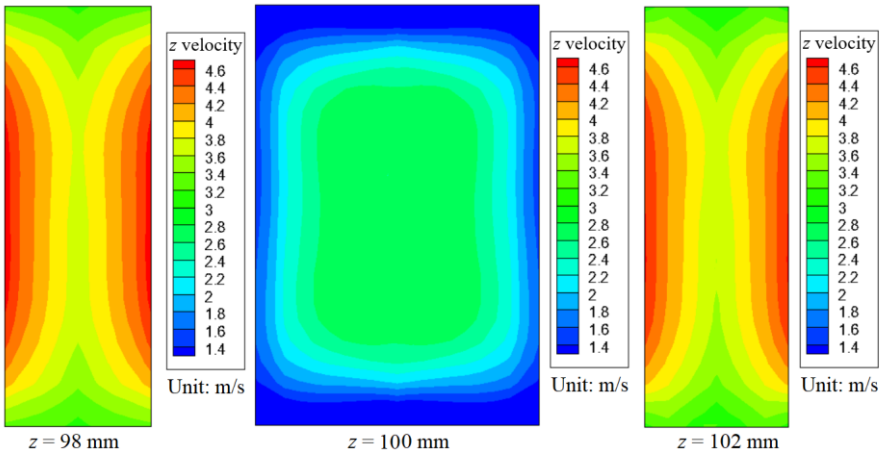

Figure 7. Velocity contours of the channel with aligned fins.

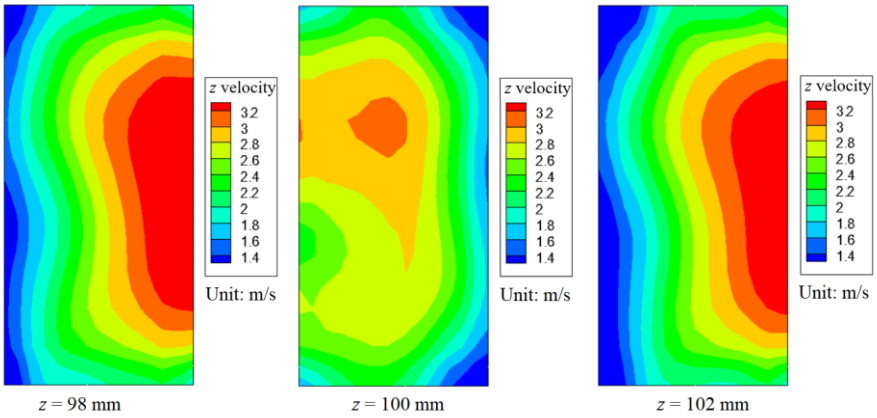

Figure 8. Velocity contours of the channel with offset fins.

Figures 9–11 show the corresponding temperature fields. For the smooth channel, strong temperature stratification is observed. The temperature at the center is significantly higher than near the walls, which indicates limited mixing and weak convective effects. In the channel with aligned fins, the flow passage geometry causes periodic constriction and expansion, which enhances turbulence and disrupts the thermal boundary layer uniformly along the flow path. As a result, the temperature distribution across the channel becomes more uniform, and the temperature gradient in the *x*-*y* plane is significantly reduced. The isotherms tend to follow the periodic geometry, and heat is more effectively transferred from the wall to the fluid, which leads to improved thermal performance. In the channel with offset fins, the staggered arrangement causes irregular flow redirection, which enhances lateral fluid motion and creates local recirculation zones. These effects break up thermal stratification more randomly than in the aligned configuration. Although this results in more complex and asymmetrical temperature fields, it also improves fluid mixing and contributes to higher convective heat transfer. However, due to the less regular disruption of the boundary layer, the reduction in the temperature gradient is less uniform than in the aligned case.

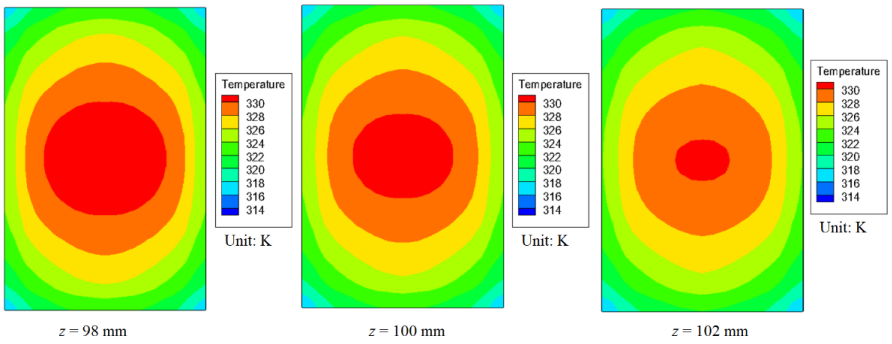

Figure 9. Temperature fields of the smooth channel.

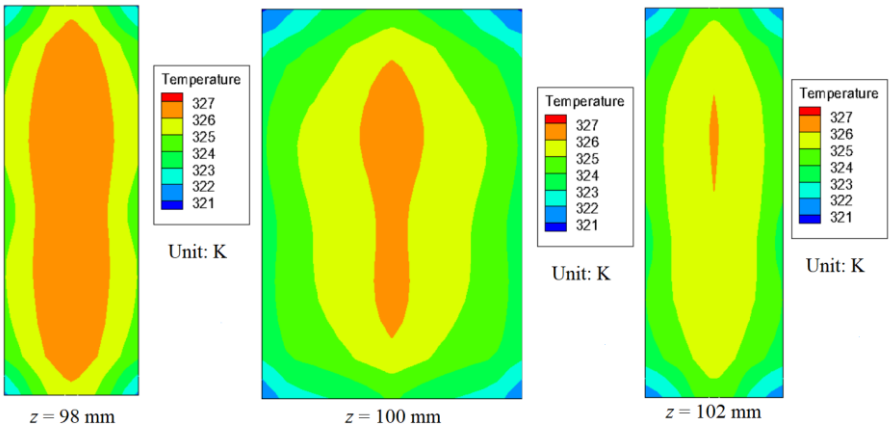

Figure 10. Temperature fields of the channel with aligned fins.

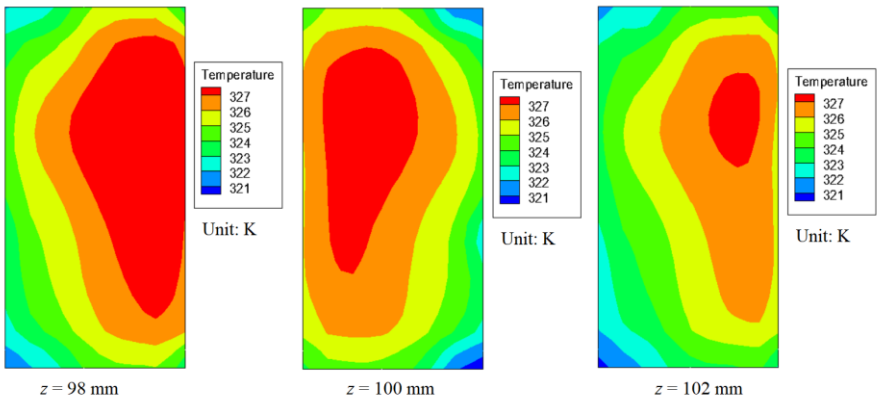

Figure 11. Temperature fields of the channel with offset fins.

4.2. Local Heat Transfer and Fluid Flow Performance

Investigating the local heat transfer performance along the channel length is essential for understanding and optimizing the thermal behavior of supercritical CO_2 flow in minichannels. Due to the strong variations in thermophysical properties near the pseudo-critical point, the local heat transfer coefficient can fluctuate significantly along the flow direction. These variations are closely linked to the evolution of fluid properties such as specific heat capacity, density and thermal conductivity, as well as changes in flow velocity and turbulence intensity. Local heat transfer analysis helps identify regions of high and low thermal performance, which is critical for designing efficient and compact heat exchangers. By investigating the local heat transfer performance, designers can optimize fin arrangements, channel dimensions and flow conditions to ensure uniform temperature distribution and high thermal effectiveness.

Figure 12 illustrates the variation of fluid temperature and its gradient along the flow direction. During the cooling process, the temperature gradient in the flow direction (z-axis) initially decreases, reaches a minimum, and then rises as the temperature continues to drop. The minimum gradient is observed when the fluid temperature is approximately 318 K. This behavior reflects the change in specific heat with temperature. Under constant heat flux conditions, a smaller temperature gradient indicates a higher specific heat capacity. At a system pressure of 100 bar, the pseudo-critical temperature is near 318 K, where the specific heat of supercritical CO_2 peaks. This maximum specific heat corresponds to the lowest temperature gradient, which occurs at around z = 145 mm.

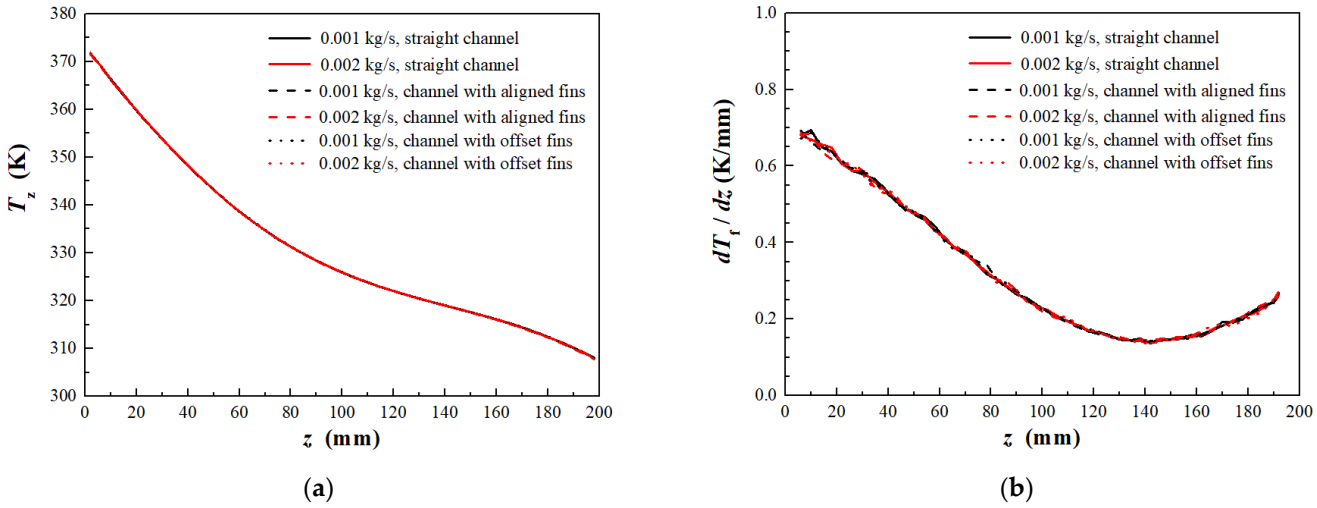

Figure 12. Local temperature and temperature gradient of fluid flow. (**a**) Local temperature; (**b**) Local temperature gradient.

As CO_2 flows through the pseudo-critical region, its thermophysical properties, including specific heat, density and viscosity, change dramatically with temperature and pressure, which makes the heat transfer process highly dependent on local conditions. Therefore, before analyzing the local heat transfer performance, Figure 13 presents the variation of the fluid properties along the flow direction. From the inlet to the outlet, fluid density increases from 189 kg/m^3 to 713 kg/m^3, while specific heat rises from 1.52 kJ/(kg·K), peaks at 8.09 kJ/(kg·K) around z = 150 mm, then decreases to 3.98 kJ/(kg·K). Thermal conductivity increases from 31.8 mW/(m·K) to 77.8 mW/(m·K), and dynamic viscosity grows from 21.9 μPa·s to 57.7 μPa·s. The rates of change in density and viscosity accelerate downstream, while thermal conductivity shows a complex trend of rising before and after the pseudo-critical region but briefly declining near it. These shifting properties have a strong impact on the local heat transfer of supercritical CO_2.

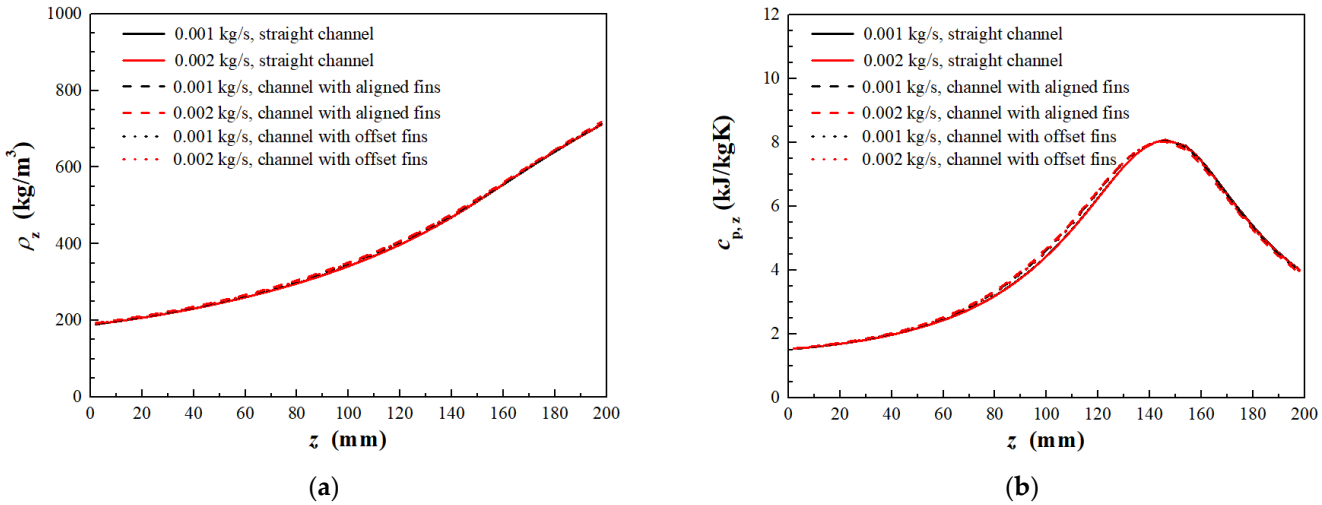

Figure 13. *Cont.*

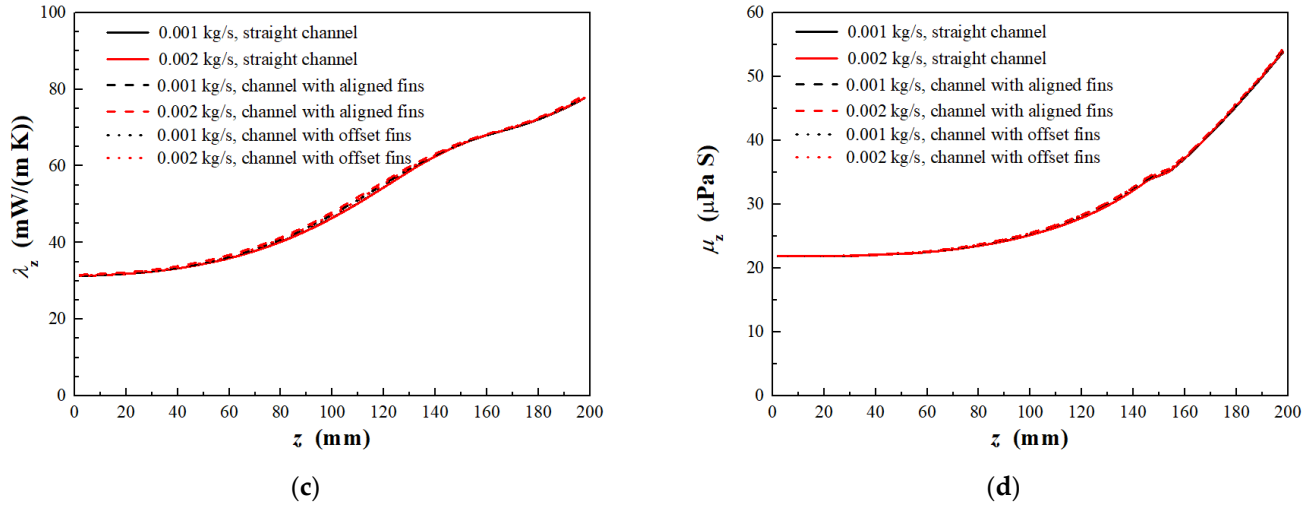

(**c**) (**d**)

Figure 13. Local fluid thermophysical properties. (**a**) Density; (**b**) Specific heat; (**c**) Thermal conductivity; (**d**) Dynamic viscosity.

Figure 14 demonstrates the local heat transfer characteristics, including the temperature difference between the bulk fluid and channel walls, the heat transfer coefficient and the Nusselt number. At any given axial position (z), the finned channels exhibit a significantly smaller wall-to-fluid temperature difference compared to the smooth channel. Among the finned designs, the channel with aligned fins shows the lowest temperature difference. In the smooth channel, increasing the mass flow rate leads to a notable rise in temperature difference. In contrast, the finned configurations, particularly the aligned fin design, show only a modest increase in temperature difference with higher flow rates. Heat transfer performance in this context is primarily influenced by how effectively energy is transported from the wall-adjacent fluid to the core flow. The introduction of fins enhances turbulence and fluid mixing and leads to a substantial improvement in convective heat transfer. At a flow rate of 0.001 kg/s and z = 150 mm, the local heat transfer coefficients are 6.7 kW/(m^2·K) for the smooth channel, 15.9 kW/(m^2·K) for the aligned fin channel and 11.5 kW/(m^2·K) for the offset fin channel. Near the pseudo-critical region, heat transfer behavior closely follows changes in specific heat capacity, which peaks around this point. As a result, the local heat transfer coefficient initially rises, reaches a maximum, and then declines downstream. It is important to note that the heat transfer peak aligns more closely with the pseudo-critical temperature near the wall rather than with the bulk temperature. The maximum heat transfer occurs at z = 130 mm, whereas the pseudo-critical bulk temperature appears around z = 145 mm. The Nusselt number, which is a function of both the heat transfer coefficient and thermal conductivity, reflects these trends. The rise in thermal conductivity downstream helps to moderate the decline in Nusselt number when the fluid temperature drops below the pseudo-critical point.

In passive heat transfer enhancement methods, an increase in pressure drop is often observed due to the added form drag and intensified fluid turbulence. Figure 15a illustrates the local pressure variation along the channel length. In the smooth channel, pressure gradually decreases, primarily resulting from frictional losses. Additionally, the pressure drops caused by deceleration during cooling are notably reduced because the fluid density and viscosity are highly sensitive to temperature changes. For channels equipped with fins, the complex geometry combined with the thermophysical properties of supercritical CO_2 near the pseudo-critical point significantly influences the flow behavior. Enhanced turbulence and fluid mixing in these channels contribute to greater energy dissipation and friction and lead to higher pressure drops. This is more pronounced for aligned fins

due to a more direct obstruction of the flow path. Furthermore, as shown in Figures 9–11, the near-wall temperature in the finned channels is higher than in the smooth channel, which lowers the density, increases near-wall velocity and further elevates the pressure drop. For mass flow rates of 0.001 kg/s and 0.002 kg/s, the aligned fin channel exhibits pressure drops of 29.1 kPa and 113.6 kPa, respectively, while the offset fin channel shows 15.5 kPa and 59.9 kPa. Figure 15b shows that the friction factor is considerably higher for finned channels compared to the smooth one, with aligned fins producing the largest values. Figure 15c demonstrates that despite the significant decrease in local Reynolds number along the flow, the friction factor remains almost constant in finned channels due to enhanced turbulence and flow structure.

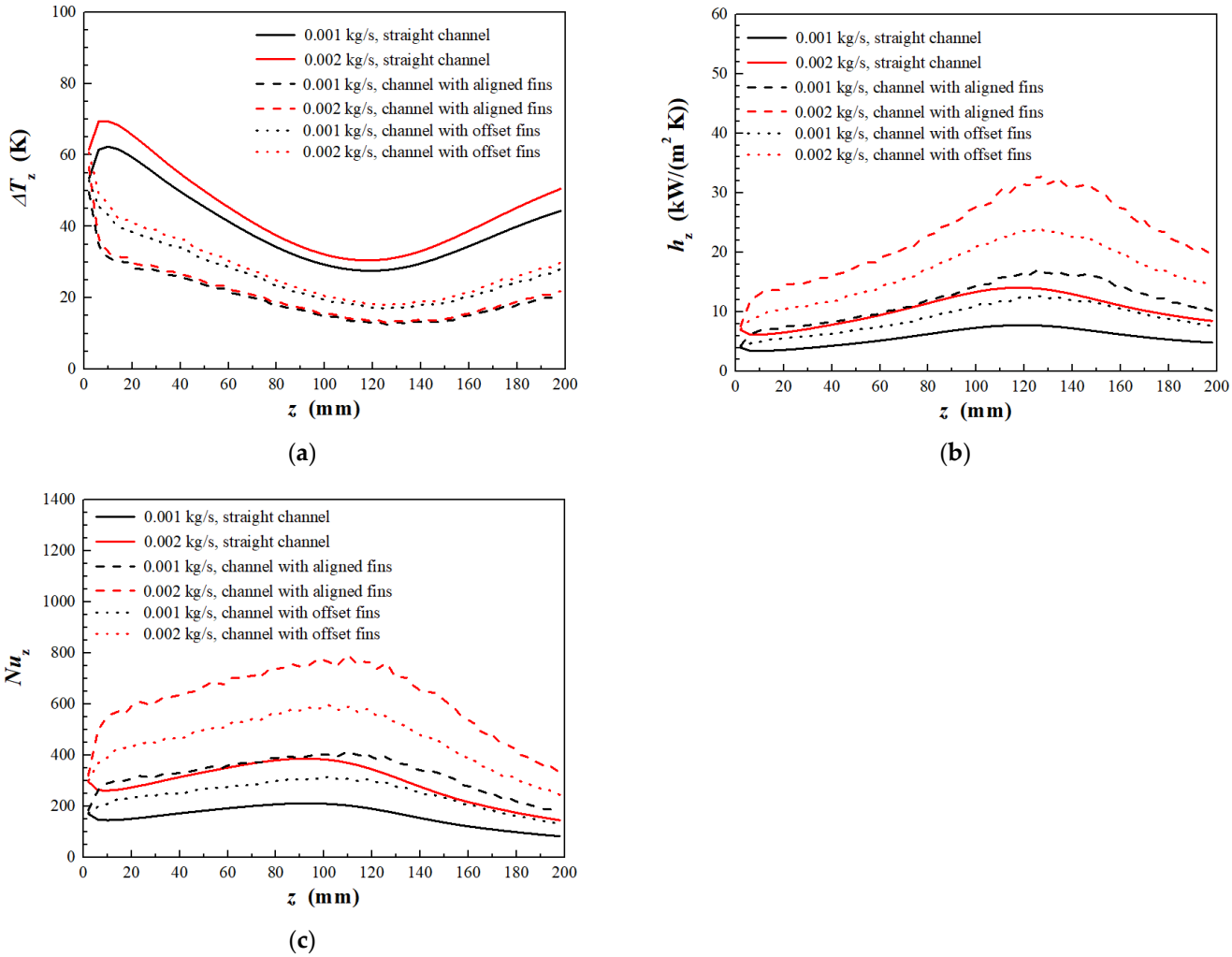

Figure 14. Local heat transfer performance. (**a**) Temperature difference between the fluid and the channel wall; (**b**) Heat transfer coefficient; (**c**) Nusselt number.

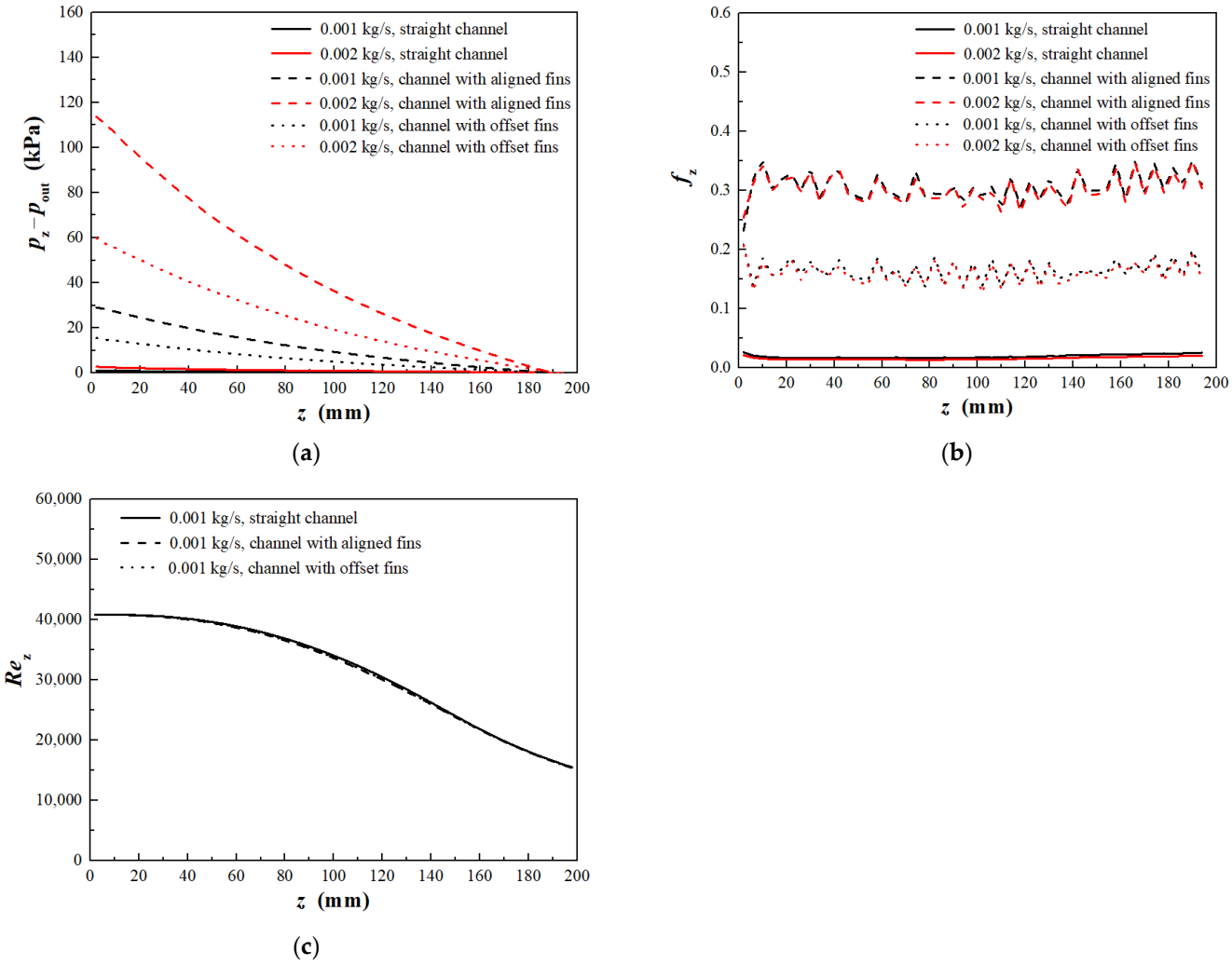

Figure 15. Local fluid flow performance. (**a**) Pressure drop; (**b**) Friction factor; (**c**) Reynolds factor.

4.3. Average Heat Transfer and Fluid Flow Performance

Unlike local measurements which capture variations at specific points, average heat transfer coefficients provide a comprehensive assessment of the system's overall thermal efficiency. These values integrate the effects of varying thermophysical properties, flow conditions and geometric features such as fins or channel shape across the entire heat exchanger length. Supercritical CO_2 exhibits rapid changes in specific heat, thermal conductivity and viscosity near the pseudo-critical point, which makes its average heat transfer behavior highly sensitive to operating pressure and temperature. Accurately evaluating the average heat transfer performance enables engineers to determine the required surface area for a given thermal duty, estimate pressure drops and assess the effectiveness of enhancement features like aligned or offset fins.

Figure 16 illustrates the average heat transfer behavior and the influence of the increasing flow rate represented by a rising Reynolds number. As the mass flow rate increases from 0.0005 kg/s to 0.003 kg/s, the corresponding mass flux rises from 333 kg/(m^2·s) to 2000 kg/(m^2·s). This increase leads to a significant improvement in the average heat transfer coefficient in the smooth channel, from 3.3 kW/(m^2·K) to 14.7 kW/(m^2·K). This improvement is primarily driven by higher flow velocity and reduced thermal boundary layer thickness. When aligned or offset fins are incorporated into the channel walls, the average heat transfer is further improved. These fins interrupt the boundary layer, generate additional flow disturbances and promote mixing in the near-wall regions, which signifi-

cantly enhance the heat transfer process. For channels incorporating aligned and offset fins, the average heat transfer coefficient rises from 6.2 kW/(m^2·K) to 33.2 kW/(m^2·K) and from 4.8 kW/(m^2·K) to 24.3 kW/(m^2·K), respectively. The better performance resulting from aligned fins over offset fins is primary from the more consistent disruption of the flow and higher turbulence levels. The corresponding Reynolds number spans from approximately 1.58×10^4 to 9.46×10^4 in the smooth channel, and it is slightly lower in finned channels due to varied temperature distributions. In terms of Nusselt numbers, the smooth, aligned-fin and offset-fin channels show increases from 91.2 to 415.3, 169.1 to 895.1 and 131.5 to 665.6, respectively, which highlights the performance gains from enhanced heat transfer mechanisms. The higher average heat transfer coefficient signifies more efficient thermal exchange between the CO_2 and the channel walls, which can lead to smaller, lighter and more cost-effective heat exchanger designs. It also supports energy-saving objectives by minimizing the temperature difference required to transfer a given amount of heat.

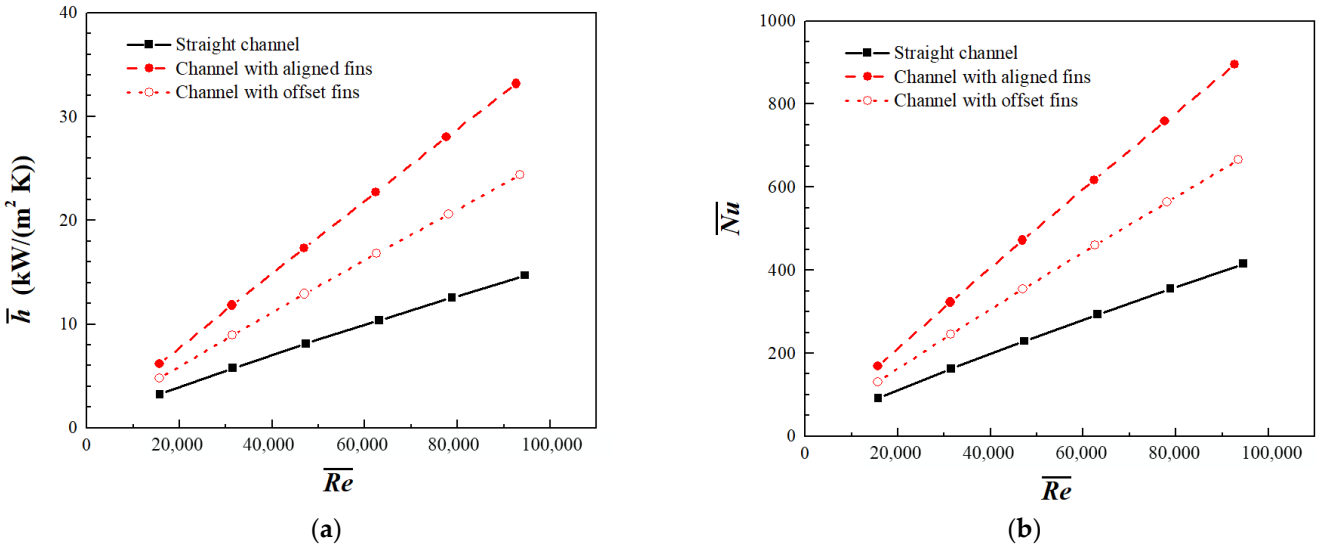

Figure 16. Average heat transfer performance. (**a**) Heat transfer coefficient; (**b**) Nusselt number.

Figure 17a illustrates how the total pressure drop varies with increasing mass flux of supercritical CO_2. The total pressure drop is influenced by both the mass flux and the channel geometry, with frictional losses typically being the primary contributors. As mass flux rises, the pressure drop generally increases significantly. Thermal conditions such as heating or cooling also affect the pressure drop through flow acceleration or deceleration. In smooth channels, flow deceleration during cooling can notably reduce the pressure drop, which mitigates the total pressure drop. For instance, when the mass flux increases from 333 kg/(m^2·s) to 2000 kg/(m^2·s), the pressure drop in the smooth channel rises only from 0.4 kPa to 4.7 kPa. In contrast, channels with fins experience much larger pressure drops due to enhanced turbulence and added form drag. For aligned fins, the pressure drops climb sharply from 7.5 kPa to 248.9 kPa, potentially increasing compressor power and affecting system efficiency. The offset fin configuration produces lower pressure drops, increasing from 4.1 kPa to 133.3 kPa. Figure 17b shows the relationship between average friction factor and Reynolds number. Integrated fins significantly elevate the friction factor, particularly in aligned configurations. While the smooth channel's friction factor decreases from 0.026 to 0.014 as the mass flux rises, the aligned and offset fin channels show minor reductions, from 0.31 to 0.28 and 0.17 to 0.15, respectively. This indicates that the Reynolds number has a limited effect on the friction factor in finned channels. It should be pointed out that if the CO_2 pressure drop in the gas cooler is a few percentage points of the high-

side pressure, its influence on the coefficient of performance (COP) of trans-critical CO_2 refrigeration and heat pump systems is generally limited. For example, a 100 kPa gas cooler pressure drop at 100 bar of high-side pressure in typical trans-critical CO_2 systems results in a 1% relative pressure drop, which involves a negligible change in system COP (often less than 0.5%).

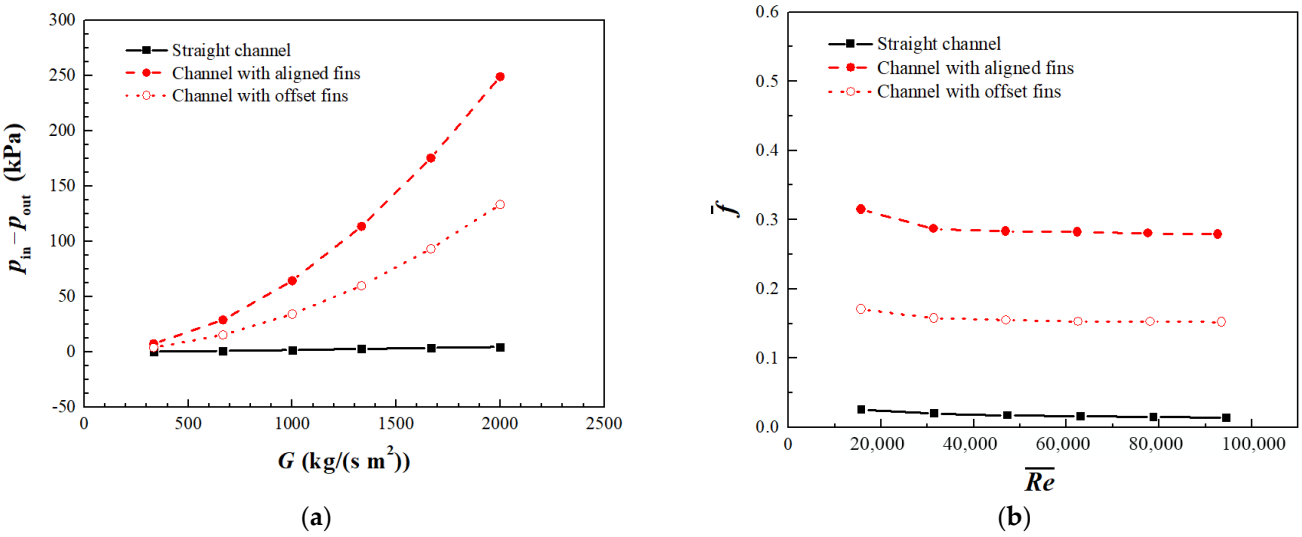

Figure 17. Average fluid flow performance. (**a**) Total pressure drops; (**b**) Average friction factor.

5. Conclusions

To enhance the heat transfer performance of minichannel gas coolers, configurations with aligned and offset fins embedded in the channel sidewalls are proposed. A detailed three-dimensional turbulence model incorporating NIST real-gas properties of supercritical CO_2 was developed to analyze the associated heat transfer behaviors. The current study focuses on both local and average heat transfer and fluid flow performance, with the temperature of CO_2 exactly decreasing from 373.15 K to 308.15 K. The key findings are summarized below:

The velocity contour and temperature distribution reveal that the heat transfer and fluid flow characteristics are significantly influenced by the fin configurations. In smooth channels, the velocity is concentrated at the center, while stagnation zones form near the walls, particularly in corners, leading to weak fluid mixing and large temperature gradients. In contrast, channels with integrated fins, especially those with aligned arrangements, promote flow disturbance, accelerate mixing and reduce temperature stratification through periodic flow constriction and expansion, thereby enhancing turbulence and overall heat transfer.

Local heat transfer performance is closely related to variations in the thermophysical properties of supercritical CO_2, particularly near the pseudo-critical region where specific heat peaks. The local heat transfer coefficient increases along the flow direction, reaching a maximum around the pseudo-critical point, and then gradually decreases as the temperature continues to drop. The presence of fins augments local turbulence and improves thermal transport near the walls, effectively reducing the temperature difference between wall and bulk fluid. Aligned fins show stronger mixing effects and deliver higher local heat transfer coefficients than offset fins. At a flow rate of 0.001 kg/s and a position of z = 150 mm, the local heat transfer coefficients are 6.7 kW/(m^2·K) in the smooth channel, 15.9 kW/(m^2·K) in the channel with aligned fins and 11.5 kW/(m^2·K) in the channel with offset fins.

Increased mass flux leads to a rise in Reynolds number and average heat transfer coefficient. Channels with aligned fins demonstrate the highest thermal enhancement. Offset fins also improve performance, but to a lesser extent. Compared to the smooth channel, the aligned-finned channel shows 1.85 to 2.15 times higher average heat transfer, while the offset-finned channel achieves 1.44 to 1.61 times enhancement. Understanding the influence of channel geometry and flow conditions on average heat transfer performance will be helpful for optimizing heat exchanger design, enabling reduced size, improved efficiency and lower operating costs in CO_2 refrigeration and heat pump systems.

The introduction of aligned or offset fins on the channel sidewalls significantly increases the pressure drop compared to smooth channels, primarily due to added form drag, enhanced turbulence and repeated flow acceleration and deceleration around the fins. However, its influence on the COP of trans-critical CO_2 refrigeration and heat pump systems is generally limited, due to the relatively small ratio of pressure drop to high-side CO_2 pressure. The Reynolds number has a limited effect on the friction factor in finned channels.

In future work, it is recommended that a systematic parametric study is conducted to quantify how fin geometry influences performance. In particular, varying fin height, spacing and cross-sectional shape should be explored to obtain their combined effects on turbulence generation, boundary-layer disruption, pressure drop and heat transfer enhancement.

Funding: This research was funded by Brunel Research Culture Seed Fund No. 13157.

Data Availability Statement: All data used are in the paper, but if any additional information is required, it can be obtained by contacting the corresponding author.

Conflicts of Interest: The authors declare no conflicts of interest.

Nomenclature

A	area, m^2
c_p	specific heat, J/(kg K)
$\overline{c_p}$	averaged specific heat over cross-section at constant pressure, J/(kg K)
D	hydraulic diameter, m
f	friction factor
$\bar{f}$	average friction factor
G	mass flux, kg/(m^2·s)
G_k	turbulence kinetic energy due to mean velocity gradients, J/kg
G_b	turbulence kinetic energy due to buoyancy, J/kg
h	heat transfer coefficient, W/(m^2·K)
$\overline{h}$	average heat transfer coefficient, W/(m^2·K)
k	turbulent kinetic energy, m^2/s^2
L	length, m
m	mass flow rate, kg/s
n	exponent in Equation (14)
Nu	Nusselt number
$\overline{Nu}$	average Nusselt number
p	pressure, Pa
$\overline{Pr_b}$	averaged Prandtl number over cross-section at constant pressure
q	heat flux, W/m^2
Q	heat transfer rate, W
Re	Reynolds number
$\overline{Re}$	average Reynolds number
SST	Shear Stress Transport
T	temperature, K

u	velocity, m/s
x, y, z	three coordinates shown in Figure 2, m
$\frac{dp_f}{dz}$	pressure gradient due to friction, Pa/m
Greek letters	
α_k	inverse effective Prandtl numbers for turbulent kinetic energy
α_ε	inverse effective Prandtl numbers for turbulent dissipation
ρ	density, kg·m^{-3}
λ	thermal conductivity, W/(m K)
ε	turbulent dissipation, m^2/s^3
μ	dynamic viscosity, Pa·s
Subscripts	
in	inlet
f	fluid
out	outlet
w	wall
z	local

References

1. Austin, B.T.; Sumathy, K. Trans-critical carbon dioxide heat pump systems: A review. *Renew. Sustain. Energy Rev.* **2011**, *15*, 4013–4029. [CrossRef]
2. Cavallini, A.; Cecchinato, L.; Corradi, M.; Fornasieri, E.; Zilio, C. Two-stage trans-critical carbon dioxide cycle optimisation: A theoretical and experimental analysis. *Int. J. Refrig.* **2005**, *28*, 1274–1283. [CrossRef]
3. Lorentzen, G. Trans-Critical Vapour Compression Cycle Device. International Patent Publication, Patent Number WO90/07683, 12 July 1990.
4. Pettersen, J.; Hafner, A.; Skaugen, G.; Rekstad, H. Development of compact heat exchangers for CO_2 air-conditioning systems. *Int. J. Refrig.* **1998**, *21*, 180–193. [CrossRef]
5. Chai, L.; Tassou, S.A. A review of heat transfer of CO_2 at supercritical pressure in the critical and pseudo-critical region. *J. Enhanc. Heat Transf.* **2022**, *29*, 1–40. [CrossRef]
6. Yin, J.M.; Bullard, C.W.; Hrnjak, P.S. R-744 gas cooler model development and validation. *Int. J. Refrig.* **2001**, *24*, 692–701. [CrossRef]
7. Asinari, P.; Cecchinato, L.; Fornasieri, E. Effects of thermal conduction in microchannel gas coolers for carbon dioxide. *Int. J. Refrig.* **2004**, *27*, 577–586. [CrossRef]
8. Ge, Y.T.; Cropper, R.T. Simulation and performance evaluation of finned-tube CO_2 gas coolers for refrigeration systems. *Appl. Therm. Eng.* **2009**, *29*, 957–965. [CrossRef]
9. Gupta, D.K.; Dasgupta, M.S. Simulation and performance optimization of finned tube gas cooler for trans-critical CO_2 refrigeration system in Indian context. *Int. J. Refrig.* **2014**, *38*, 153–167. [CrossRef]
10. Marcinichen, J.B.; Thome, J.R.; Pereira, R.H. Working fluid charge reduction. Part II: Supercritical CO_2 gas cooler designed for light commercial appliances. *Int. J. Refrig.* **2016**, *65*, 273–286. [CrossRef]
11. Chai, L.; Tsamos, K.M.; Tassou, S.A. Modelling and evaluation of the thermohydraulic performance of finned-tube supercritical carbon dioxide gas coolers. *Energies* **2020**, *13*, 1031. [CrossRef]
12. Zendehboudi, A.; Ye, Z.; Hafner, A.; Andresen, T.; Skaugen, G. Heat transfer and pressure drop of supercritical CO_2 in brazed plate heat exchangers of the tri-partite gas cooler. *Int. J. Heat Mass Transf.* **2021**, *178*, 121641. [CrossRef]
13. Chu, W.; Li, X.; Chen, Y.; Wang, Q.; Ma, T. Experimental study on small scale printed circuit heat exchanger with zigzag channels. *Heat Transf. Eng.* **2021**, *42*, 723–735. [CrossRef]
14. Ren, Z.; Zhang, L.; Zhao, C.-R.; Jiang, P.-X.; Bo, H.-L. Local Flow and Heat Transfer of Supercritical CO_2 in Semicircular Zigzag Channels of Printed Circuit Heat Exchanger during Cooling. *Heat Transf. Eng.* **2021**, *42*, 1889–1913. [CrossRef]
15. Zhu, Y.; Huang, Y.; Lin, S.; Li, C.; Jiang, P. Study of convection heat transfer of CO_2 at supercritical pressures during cooling in fluted tube-in-tube heat exchangers. *Int. J. Refrig.* **2019**, *104*, 161–170. [CrossRef]
16. Ye, Z.; Wang, Y.; Zendehboudi, A.; Hafner, A.; Cao, F. Investigation on the performance of fluted tube-in-tube gas cooler in trans-critical CO_2 heat pump water heater. *Int. J. Refrig.* **2022**, *135*, 208–220. [CrossRef]
17. Fronk, B.M.; Garimella, S. Water-coupled carbon dioxide microchannel gas cooler for heat pump water heaters: Part I—Experiments. *Int. J. Refrig.* **2011**, *34*, 7–16. [CrossRef]
18. Fronk, B.M.; Garimella, S. Water-coupled carbon dioxide microchannel gas cooler for heat pump water heaters: Part II—Model development and validation. *Int. J. Refrig.* **2011**, *34*, 17–28. [CrossRef]

19. Yang, Y.; Li, M.; Wang, K.; Ma, Y. Study of multi-twisted-tube gas cooler for CO_2 heat pump water heaters. *Appl. Therm. Eng.* **2016**, *102*, 204–212. [CrossRef]
20. Chen, Z.; Li, Q.; Meier, D.; Warnecke, H.-J. Convective heat transfer and pressure loss in rectangular ducts with drop-shaped pin fins. *Heat Mass Transf.* **1997**, *33*, 219–224. [CrossRef]
21. Wang, F.; Zhang, J.; Wang, S. Investigation on flow and heat transfer characteristics in rectangular channel with drop-shaped pin fins. *Propuls. Power Res.* **2012**, *1*, 64–70. [CrossRef]
22. Bai, J.; Pan, J.; He, X.; Wang, K.; Tang, L.; Yang, R. Numerical investigation on thermal hydraulic performance of supercritical LNG in sinusoidal wavy channel based printed circuit vaporizer. *Appl. Therm. Eng.* **2020**, *175*, 115379. [CrossRef]
23. Chai, L.; A Tassou, S. Effect of cross-section geometry on the thermohydraulic characteristics of supercritical CO_2 in minichannels. *Energy Procedia* **2019**, *161*, 446–453. [CrossRef]
24. Krasonshchekov, E.A.; Protopopov, V.S. Experimental study of heat exchange in carbon dioxide in the supercritical range at high temperature drops. *High. Temp.* **1966**, *4*, 375–382.
25. Jackson, J. Fluid flow and convective heat transfer to fluids at supercritical pressure. *Nucl. Eng. Des.* **2013**, *264*, 24–40. [CrossRef]
26. Petukhov, B.S. About heat transfer at turbulent fluid flow in tubes. *Therm. Eng.* **1958**, *4*, 63–68.